Density-functional-theory investigation of conformations, ^{13}C shielding, and magnetic field interactions in a V-shaped phenylene bis carboxylate homologous series

Alberto Marini*
Dipartimento di Chimica e Chimica Industriale, Universitá di Pisa, via Risorgimento 35, I-56126 Pisa, Italy

Ronald Y. Dong†
Department of Physics and Astronomy, University of British Columbia, Vancouver, British Columbia, Canada V6T 1Z1
(Received 13 November 2010; published 29 April 2011)

Density functional theory (DFT) has been employed in a conformational study of a bent-core PBBC homologous series. IR spectra, GIAO-DFT chemical shielding tensors (CSTs), and molecular susceptibility tensors (MSTs) are theoretically calculated for various optimized conformations established by searching the potential energy surface of each PBBC V-shaped molecule. The IR results could aid the understanding of vibration normal modes, while the MST results can illuminate the alignment properties of the V-shaped molecules in an external magnetic field. CSTs of the aromatic carbons, and those previously measured by the 2D-NMR SUPER technique (with some ^{13}C NMR peaks reassigned for correctness based on new DFT calculations), were found to be in good agreement. These verified experimental CSTs are then used to revisit the ^{13}C NMR data to yield structural and local orientational order parameters for two members of the PBBC series. The PBBC series studied using the combined DFT-^{13}C NMR approach strongly supports the notion that lesser populated conformational states found by DFT could be reached in the studied mesogens 10DClPBBC and 11ClPBBC upon decreasing temperature, as revealed by the change in the bend angle determined by NMR and identified with those of the DFT molecular structures optimized for various conformers.

DOI: 10.1103/PhysRevE.83.041712 PACS number(s): 61.30.Gd, 71.15.Mb, 82.56.−b, 75.30.Cr

I. INTRODUCTION

The homologous PBBC series (1,3-phenylene bis[4′-alkenyloxy biphenyl]-4-carboxylate derivatives) has been studied [1] by means of ^{13}C NMR chemical shifts to determine the local order parameter tensor **S** of each aromatic fragment within the V-shaped molecular cores. The difference in the local (molecular) biaxiality Δ values for various fragments within the aromatic region of the V-shaped molecule A131 was found to be essential in determining its possible conformations [2–4]. A131 is known to exhibit a uniaxial to biaxial nematic transition [5]. The existence of a biaxial nematic phase (N_b) in V-shaped molecules has been a controversial subject ever since the rediscovery of liquid crystals (LC) composed of bent-core (or V-shaped) molecules [6]. The phase biaxiality in a biaxial nematic of D_{2h} symmetry is described by the biaxial order parameters P and C [7], which vanish in the uniaxial nematic (N_u) phase but are nonzero in the N_b phase [8]. When the nematic director is aligned along the external magnetic field, it is known that even in the biaxial nematics the phase biaxial order parameters are not detectable [9]. Even though the present PBBC series, to our best knowledge, does not possess any biaxial nematic phase, it can be used to further test the approach employed for A131, that is, to verify the carbon peak assignments in both the isotropic and nematic phases, as well as to assess the quality of experimentally observed carbon chemical shift powder patterns previously reported in the PBBC series, viz., to compare them with the DFT computed chemical shielding tensors for various conformations. In fact, the current analyses of the reported ^{13}C chemical shifts [1] using instead the verified experimental chemical shift anisotropy (CSA) tensors did show minor variations in the derived local order parameters S and Δ. One structural factor of V-shaped molecules is the bend angle Θ subtended by the two lateral wings next to the central ring. This angle can be estimated from the derived local S values, and also obtained from the DFT determined molecular structure. The Θ angle could be one of many involved in the formation of the elusive biaxial nematics [10,11].

In this DFT study of PBBC series, optimized molecular conformations are found first by searching the potential energy surface (PES). Theoretical IR spectra, chemical shielding tensors (CSTs), and molecular susceptibility tensors (MSTs) are calculated for these conformations and discussed by comparing with those of A131 and conventional calamitics. The paper is organized as follows. Section II contains experimental and computational details. Section III reports the results and discussion under the headings (A) conformational analysis, (B) infrared spectra, (C) magnetic susceptibility, and (D) ^{13}C chemical shielding tensor and NMR analyses. Finally, a brief summary is given in Sec. IV. The DFT theory of calculating CSTs, IR frequencies, MSTs, and conformational states *in vacuo*, together with the necessary formulas used for calculating the observed ^{13}C shifts, has been detailed elsewhere [2,12].

II. EXPERIMENTAL AND COMPUTATIONAL DETAILS

The three investigated PBBC samples [e.g., see 4,6-dichloro-1,3-phenylene bis[4′-(9-decenyloxy)-1,1′-biphenyl] carboxylate; 10DClPBBC in Fig. 1(a)] have the following transition temperatures [1] in °C:

(1) 11ClPBBC: K–(63.2)–SmC–(77.6)–N_u–(84.5)–I,

(2) 10DClPBBC: K_1–(51.9)–K_2–(72.7)–K_3–(87.6)–N_u–(98.8)–I,

(3) 10BrPBBC: K–(62.0)–N_u–(70.0)–I.

*Deceased.
†rondong@phas.ubc.ca

 ©2011 American Physical Society

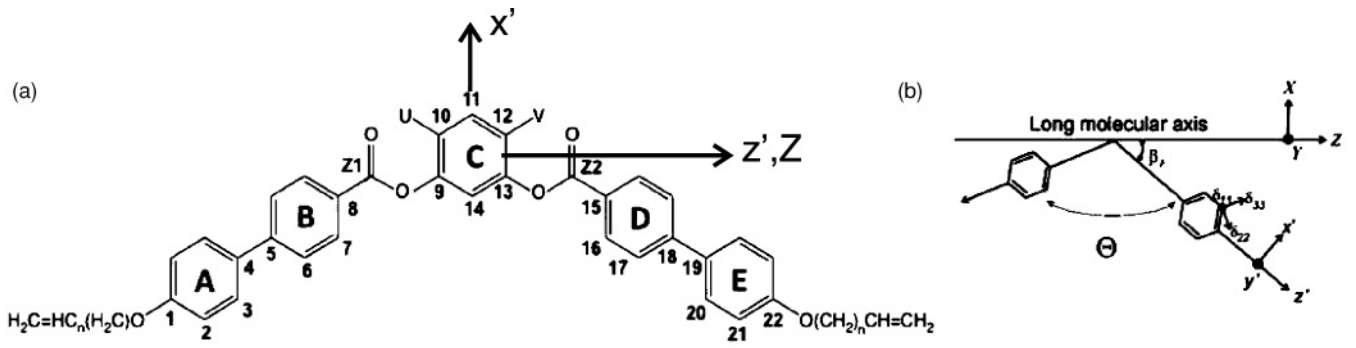

FIG. 1. (a) Molecular structure of PBBC series: 11ClPBBC ($n = 11, U = \mathrm{Cl}, V = \mathrm{H}$), 10DClPBBC ($n = 10, U = \mathrm{Cl}, V = \mathrm{Cl}$), 10BrPBBC ($n = 10, U = \mathrm{Br}, V = \mathrm{H}$). (b) Schematic of a CSA (δ_{33}, δ_{22}, δ_{11}) PAS frame, a fragment (x', y', z'), and a molecular frame (X, Y, Z) fixed on the molecule.

DFT calculations have been performed using the Gaussian 03 package [13], where all the molecular models represented in Fig. 2 are built by means of the GaussView 4.1 program. The DFT approach (with a suitable choice of both functional and basis sets), which has a computational cost of the same order as Hartree Fock (HF), and considerably less than traditional correlation techniques, often gives quality calculations comparable to or even better than those of MP2 [14]. Moreover, the DFT method is generally preferred in view of its smaller sensitivity to the basis set and in particular of its computational convenience. The experimental NMR work of PBBC mesogens [1] is addressed by utilizing a computational strategy to derive reliable theoretical ^{13}C CSTs, as demonstrated in A131, for the energy minimized conformers found during the conformational analysis.

The most populated conformational states within the five-ring (5R) molecular core were obtained via *in vacuo* DFT calculations employing the B3LYP [15–17] functional. The magnetic properties of each system were calculated *in vacuo* at the GIAO (gauge including atomic orbitals) [18] DFT level of theory. In particular, for the calculation of MSTs, we have decided to adopt the CSGT (continuous

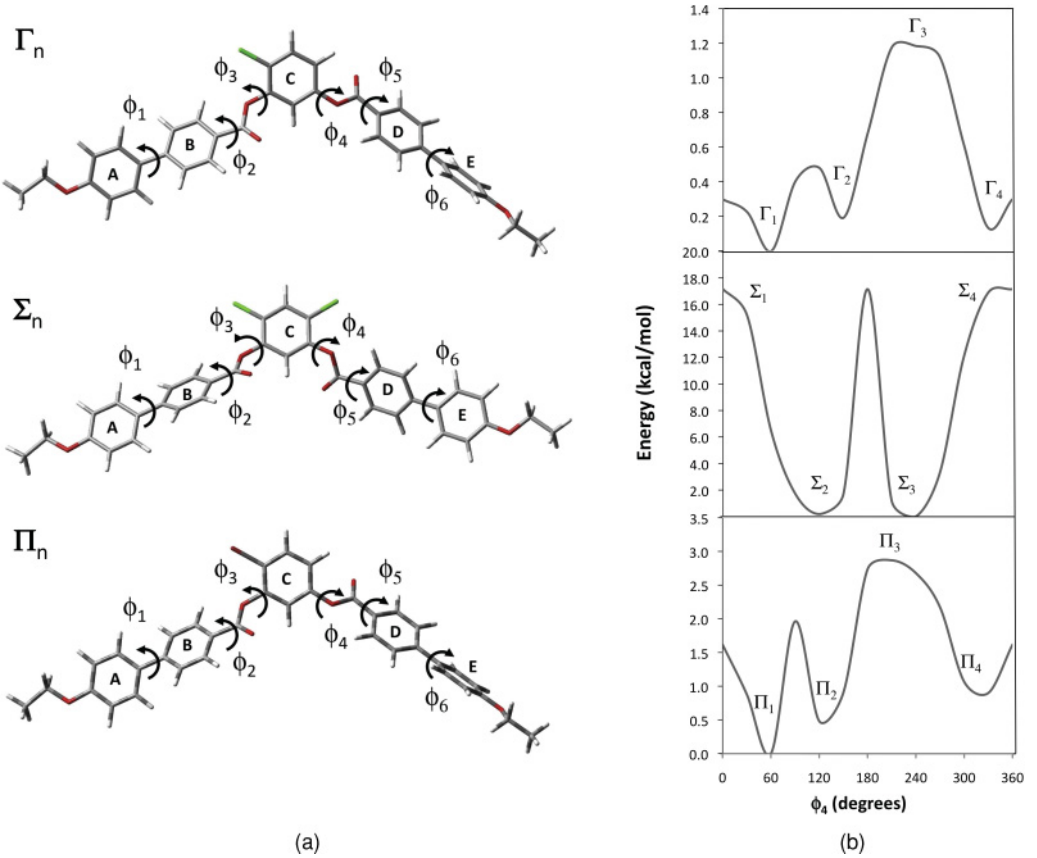

FIG. 2. (a) Molecular structures and relevant dihedral angles of three five-ring models: 2ClPBBC (Γ_n), 2DClPBBC (Σ_n), and 2BrPBBC (Π_n). (b) Energy profiles (kcal/mol) of the PES relative to dihedral angle ϕ_4.

TABLE I. Structural parameters: dihedral and bend angles (degrees), relative energies (kcal/mol), and populations (%) at $T = 300$ K for fully relaxed Γ_i, Σ_i, and Π_i conformers of the 2ClPBBC, 2DClPBBC, and 2BrPBBC 5-ring models, respectively.

Conformation	ϕ_1 (deg)	ϕ_2 (deg)	ϕ_3 (deg)	ϕ_4 (deg)	ϕ_5 (deg)	ϕ_6 (deg)	Θ (deg)	ΔE (kcal/mol)	P (%)
Γ_1	35.2	0.5	140.3	46.6	1.0	35.7	123.5	0.000	45.6
Γ_2	34.4	0.6	143.2	136.5	0.5	35.3	128.6	0.599	16.7
Γ_3	33.8	0.4	139.3	233.4	0.7	34.8	131.4	1.300	5.1
Γ_4	33.9	0.2	142.7	319.8	0.9	35.2	122.9	0.199	32.6
Σ_1	35.3	0.8	141.2	43.9	0.7	34.3	121.7	16.599	0.0
Σ_2	33.9	0.5	140.7	135.3	0.8	35.9	130.1	0.000	69.8
Σ_3	34.7	0.3	142.5	230.6	0.4	36.2	129.4	0.500	30.2
Σ_4	33.2	0.1	141.6	322.9	0.5	34.3	123.2	18.293	0.0
Π_1	37.2	0.2	141.3	47.5	0.6	34.9	124.6	0.000	63.6
Π_2	36.4	0.5	141.6	135.2	0.4	36.2	127.2	0.710	19.6
Π_3	38.3	0.2	140.5	230.6	0.8	35.3	129.4	3.397	0.2
Π_4	37.9	0.3	141.7	321.4	0.3	36.1	126.3	0.821	16.6

set of gauge transformations) method, employing the hybrid functional MPW1PW91. Both in these calculations and in various geometry optimizations, the basis set used for carbon, oxygen, and hydrogen atoms was 6-311+G(d,p), while for chlorine and bromine atoms it was LANL2DZ (Los Alamos National Laboratory effective core potentials with a double-ζ valence). Geometries obtained in this way are at least as good as, and in several cases, such as phenyl-benzoate, better than, those obtained with the Möller Plesset theory [MP2/6-31G(d)] level [19].

The IR frequencies were calculated for the energy minimized conformations at the same level of theory used for the geometry optimization. In particular, the Gaussian output files were processed by a utility function in the GaussView program that extracted fundamental frequencies and corresponding IR intensities to simulate the calculated IR spectra as a sum of Lorentzian functions. In this case, the simulated IR bands had 10 cm^{-1} bandwidths (full width at half height).

Chemical shielding tensor calculations were performed using the following hybrid functionals, which included a mixture of Hartree-Fock exchange with DFT exchange-correlation: (a) the Becke one-parameter hybrid functional B1LYP [20]; (b) the Becke three-parameter hybrid functional B3PW91, which uses the Becke exchange functional [21] and the Perdew-Wang 91 [22] correlation functional; (c) the modified Perdew-Wang [22] exchange-correlation functional, called MPW1PW91 [23], and (d) the parameter-free hybrid functional PBE1PBE (known in the literature as PBE0) [24], which used 25% exchange and 75% correlation. Finally, since a suitable choice for referencing is required to relate the carbon chemical shielding values (σ scale) and NMR chemical shifts (δ shift scale), the above mentioned functionals were used to calculate the corresponding chemical shielding σ^{ref} of TMS (tetramethylsilane) [3].

III. RESULTS AND DISCUSSION

A. Conformational analysis

Table I lists the structural parameters: dihedral and bend angles (in degrees), relative energies (in kcal/mol), and populations (in %) at $T = 300$ K for fully relaxed Ω_i conformers of the 5R models for 2ClPBBC (Ω=Γ), 2DClPBBC (Ω=Σ), and 2BrPBBC (Ω=Π). The PBBC series is characterized by having one or two halogen atoms (Cl or Br) in the central ring C, placed in the ortho position with respect to one of the lateral chains. Figure 2 shows the structures of the PBBC molecular models together with the energy profile as a function of the dihedral angle ϕ_4, which can be considered a sensible coordinate for investigating the PES of these systems.

As put in evidence in the relative populations among the different conformers reported in Table I, these halogen atoms cause a partial (or total) restriction of lateral chain rotations, due to their steric hindrance and to electronic repulsions with the C=O groups. It is possible to distinguish two different conformational groups in the PBBC series by observing the relative orientations of the two C=O groups bonded to the central ring via an oxygen atom.[1] In the antiparallel orientation (conformers $\Omega_{1,4}$) and in the parallel orientation (conformers

[1]Note that the carboxylic group COO is here distinguished in two separated subgroups, C=O and O, for convenience.

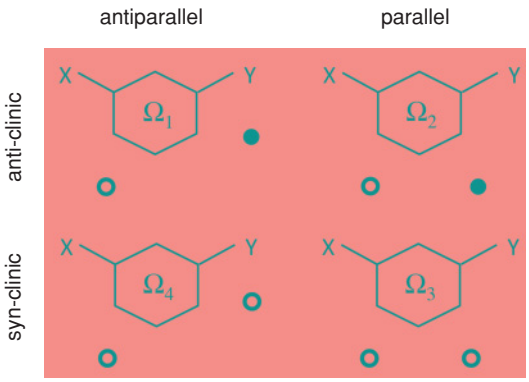

FIG. 3. (Color online) Schematic representation of the eight symmetry related conformations found for the central ring of the PBBC models discussed in the text. The hexagon stands for the central ring C, while the circles stand for the carboxylic (COO) sp^2 carbons. Moreover, the open (○) and filled (●) symbols represent above and below positions of the two sp^2 carbons with respect to the aromatic plane of ring C, respectively.

$\Omega_{2,3}$) the two C=O are oriented toward the opposite or the same direction in the phase space, respectively (see Fig. 3 and Table I). In all three cases, the highest populated conformation is the one that places the C=O groups in the anticlinic position, or in other words, the two groups with the carbonylic oxygen are on the opposite side in the phase space (e.g., conformations Γ_1, Σ_2, Π_1). The presence of one halogen atom in the central ring (Cl or Br) makes the least populated conformational states take the parallel/syn-clinic orientation for the two C=O groups, with a total population of 5.1% and 0.2% for 2ClPBBC (Γ_3) and for 2BrPBBC (Π_3), respectively. Moreover, there is a large difference in the relative energies (ΔE) ratio of Ω_2 and Ω_4 between 2ClPBBC ($\approx$3) and 2BrPBBC ($\approx$0.9). Instead, in the case of 10DClPBBC, the conformers with parallel orientation of the two C=O groups are the only ones populated at 300 K (100%). In particular, it is worth noticing that the antiparallel conformations ($\Omega_{1,4}$) always have smaller Θ angle values than the parallel ones ($\Omega_{2,3}$). This aspect will be further discussed in relation to the bend-angle values experimentally determined through the fragmental order parameters (see Sec. III D).

As far as the structural parameters are concerned, those found in the PBBC series are comparable with those determined in other bent-shape mesogens previously investigated [2,3,12,25]. In particular, the high-energy rotational barriers found for 10DClPBBC can play a central role in establishing two different conformational families as seen in a recently investigated A131 mesogen [2,3,12]. The rotational restriction introduced by the presence of halogen atoms in the PBBC series can be contrasted with A131 in which this was due to a methyl group placed in the central ring (always in the ortho position with respect to the two lateral chains).

In Fig. 4, normalized Boltzmann population (%) profiles are shown as a function of temperature (K) for the three investigated PBBC molecular models. In all cases equal distribution of conformational populations is reached at very high temperature (almost above 5000 K), while in the mesomorphic temperature range (between 330 and 390 K) the distributions should more closely reflect the energy profiles of Fig. 2(b). However, it should be emphasized here that these population profiles are derived *in vacuo*. In real LC systems, these profiles could change significantly due to collective and packing effects among molecules. In particular, the 2DClPBBC model has the highest rotational barrier along the ϕ_4 coordinate, thus leading to higher shape persistency than the other two models, 2ClPBBC and 2BrPBBC. Even in 2DClPBBC, the population of the conformers Σ_1 and Σ_4 (0% in the range 330–390 K) could increase at the expense of the most populated Σ_2 and Σ_3 conformational states. On the contrary, all three (four) conformational states are already populated in the LC range 330–390 K due to the lower energy barriers for the other two models 2ClPBBC and 2BrPBBC, in particular more so for the latter.

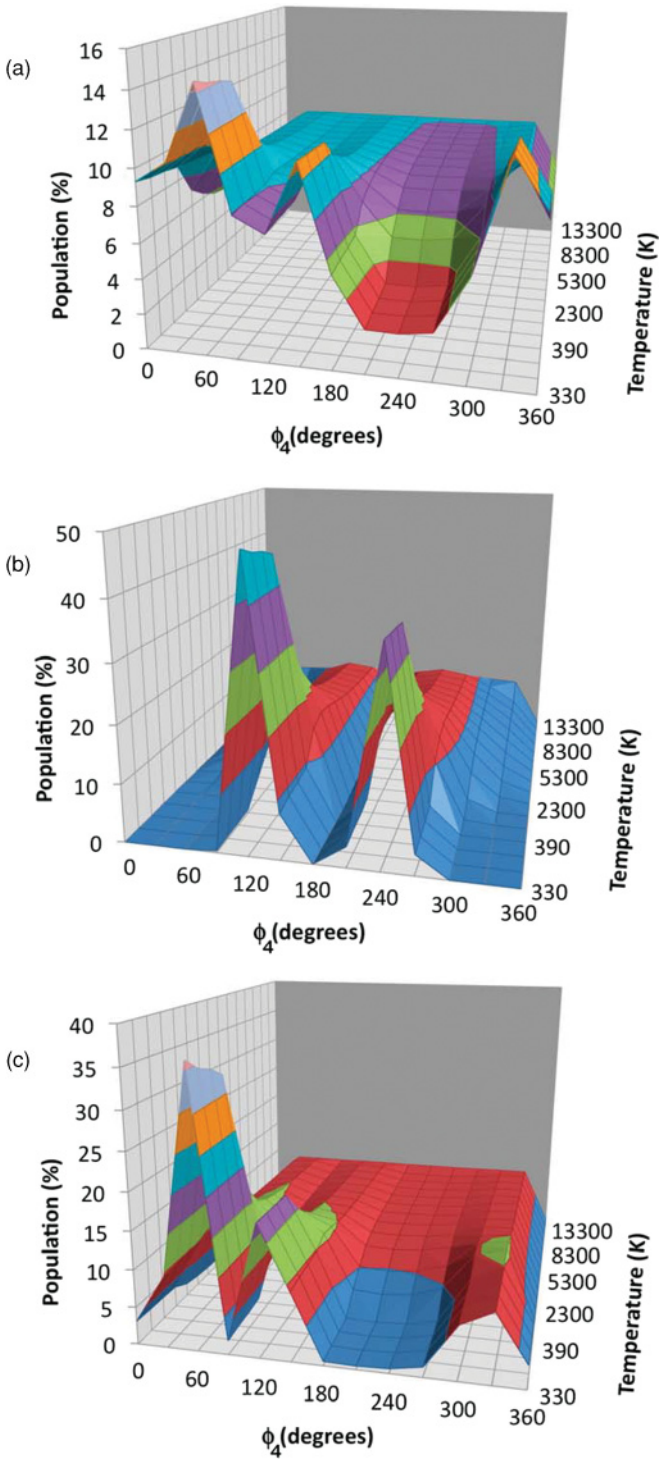

FIG. 4. (Color online) Boltzmann population (%) profiles as a function of temperature (K) for the three investigated PBBC molecular models: (a) 2ClPBBC, (b) 2DClPBBC, and (c) 2BrPBBC.

B. Infrared spectra

The *in vacuo* DFT calculated IR spectra of the three minimum energy conformers 2ClPBBC (Γ_1), 2DClPBBC (Σ_2), and 2BrPBBC (Π_1) are shown in Fig. 5. From this figure it is evident that the frequencies and intensities of the calculated IR spectra depend on the molecular structure, but the differences observed in the PBBC homologous series are very few (see the expansion of Fig. 5), practically leading to almost coincident IR spectra. A complete vibrational assignment of the calculated (and opportunely scaled according to Ref. [26]) IR harmonic frequencies has been performed and is reported in Table II for both the fingerprint (500–1200 cm^{-1}) and the functional group (1200–3200 cm^{-1}) regions, respectively.

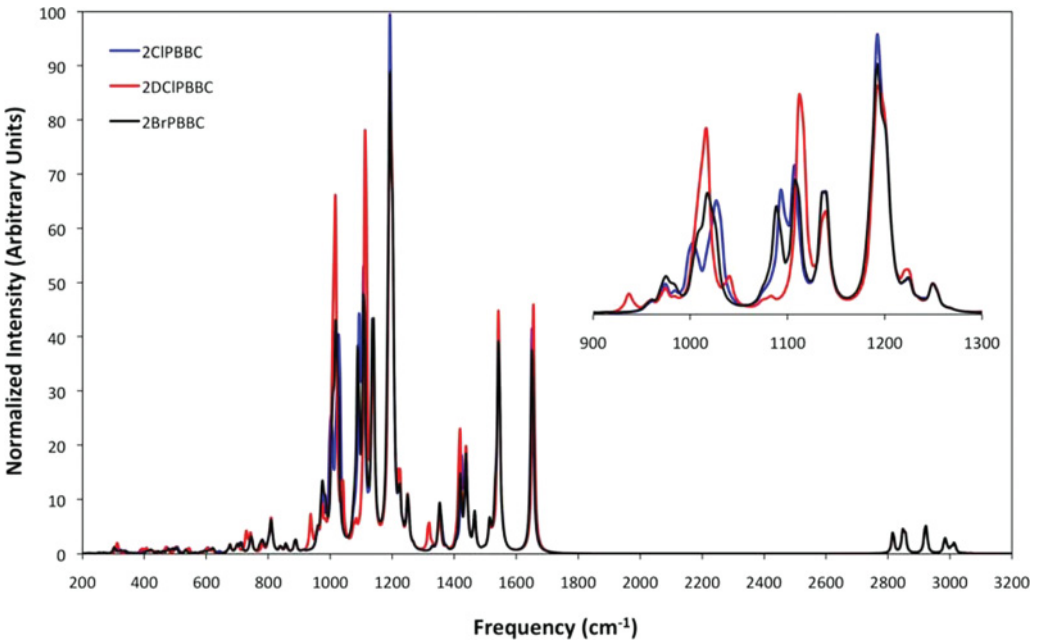

FIG. 5. (Color online) Comparison between *in vacuo* IR spectra calculated at B3LYP/6-31G(d) level of theory for the three five-ring models investigated, 2ClPBBC (Γ_1) (blue), 2DClPBBC (Σ_2) (red), and 2BrPBBC (Π_1) (black), in their lowest minimum energy conformational states. The intensity on the *y* axis is in arbitrary units. The expansion of the low-frequency region 900–1300 cm^{-1} is reported in the inset.

The current vibrational study of the low-energy region aims to elucidate the skeletal normal modes. In particular, stretching or bond angle distortion has a higher participation in describing the normal mode. Differences between theoretical and experimental IR spectra, when available, could be used to elucidate the presence of possible intermolecular effects in both the crystalline and LC phases. It is anticipated that intermolecular effects could result in distortions of the overall molecular vibration according to the symmetry of the LC phase. Moreover, several IR bands could be of potential interest for the analysis of alignment properties of PBBC mesogens [27] leading to the determination of orientational order: (i) the phenyl C=C stretching vibrations in the range of 1300–1600 cm^{-1}, (ii) the phenyl CH out-of-plane vibrations (wagging modes) within 700–900 cm^{-1}, and (iii) the symmetric stretching of carbonyl units in the range of 1600–1700 cm^{-1}. In fact, transition dipole moments for the C=C stretching vibrations (~1550 cm^{-1}) are oriented parallel to the core plane, while the transition dipole moment for the CH out-of-plane vibration (~800 cm^{-1}) is oriented perpendicular to the core plane. Thus, IR bands of the phenyl C=C stretching and the phenyl CH out-of-plane vibrations are the most sensitive indicators of ordering of the aromatic rings as their intensities are directly correlated with the core-core order. We hope that the calculated IR spectra for the main conformational states of PBBC series could induce further experimental IR work to decide on the possible shapes assumed by these mesogens in their nematic phases.

TABLE II. DFT calculated IR frequencies (cm^{-1}) (opportunely scaled for the factor 0.9613, according to Ref. [26]) and intensities in arbitrary units (arb. units) for 2ClPBBC, 2DClPBBC, and 2BrPBBC in their lowest minimum energy conformational states. The IR frequencies correspond to the theoretically assigned normal modes $\tilde{\nu}$, labeled with the following abbreviation: ν, stretching; δ, bending; ω, wagging; γ, out-of-plane bending; ρ, rocking; τ, torsion. A,B,C,D,E refer to the aromatic rings labeling.

	2ClPBBC		2DClPBBC		2BrPBBC	
Assignment	Frequency (cm^{-1})	$\tilde{\nu}$ Intensity (arb. units)	Frequency (cm^{-1})	$\tilde{\nu}$ Intensity (arb. units)	Frequency (cm^{-1})	$\tilde{\nu}$ Intensity (arb. units)
ω CH (D,E)	806.5	5.6	804.8	5.7	805.6	5.4
δ CH (B,C,D)	1012.4	39.8	1008.3	65.3	1009.6	42.2
δ CH (C)	1092.5	42.4	1128.3	78.6	1085.6	45.1
δ CH (C) + ν C-O (C)	1015.4	42.1	1148.3	39.3	1012.6	38.3
δ CH (C) + ν C-O (C)	1205.4	100.0	1203.2	83.2	1206.7	89.2
δ CH (B,D) + ν_{as} C=C (C)	1342.8	9.1	1341.7	9.4	1343.5	9.2
ν_s C=C (A,B,D,E) + ω CH (CH_2)	1521.9	37.2	1523.4	44.6	1523.6	39.8
δ CH (A,B,D,E) + ν_s C=O	1630.4	41.8	1631.4	45.3	1630.1	39.7
ν_s CH (CH_2, CH=CH_2)	2921.6	4.2	2921.5	4.3	2921.4	4.1

C. Magnetic susceptibility tensor calculations

One of the most fascinating and interesting aspects in bent-core LC concerns their organization and packing in the bulk phase, especially in the presence of an external magnetic field. The anisotropy $\Delta\chi^{\rm mol}$ of the molecular magnetic susceptibility tensor $\chi^{\rm mol}$ (MST) is strictly dependent on the molecular conformation. Since the orientation of bent-core molecules in a magnetic field is intimately related to their average molecular conformation [28,29], knowing the MST anisotropy $\Delta\chi^{\rm mol}$, although from a theoretical point of view, could be helpful to see how the mesophase director(s) orients with respect to the magnetic field. Usually, this single-molecule interaction field is not strong enough to orient a molecule or isolated molecules. However, the interaction energy due to cooperative molecular ordering is indeed crucial in generating the domain alignment [30]. In addition, the molecular MST is much different from the phase magnetic susceptibility in bulk LC, which is a quantity averaged over all motions of molecules in the LC phase. All this considered, however, the symmetry properties of the MST can help in understanding the differences, at a molecular level, in a homologous series of bent-core liquid crystals, mainly different in the central ring substitution.

At a macroscopic level, the magnetic energy density of the system can be expressed as $g_M = -\chi_a(\vec{H}\cdot\vec{n})^2/(2\mu_0)$, where μ_0 is the universal permittivity in vacuum, and χ_a is the anisotropy of the magnetic susceptibility, defined as $\chi_a = \chi_\parallel - \chi_\perp$, with $\chi_\parallel$ and $\chi_\perp$ denoting components of the phase magnetic susceptibility tensor parallel and perpendicular to the nematic director, respectively. The direction of preferred alignment of a LC system in the magnetic field depends on the sign of χ_a. Positive χ_a values seen in most LC result in the alignment of the phase director $\vec{n}$ parallel to the magnetic field $\vec{H}$; on the contrary, LC of negative χ_a values, often seen in discotic and calamitic liquid crystals constituted only of aliphatic parts, produce director alignment normal to the $\vec{H}$. The case of V-shaped molecules is less obvious, since the molecular shape of these molecules is in a way intermediate between the previous cases [28]. This makes it difficult to properly choose the direction of the long molecular axis, which could explain why certain V-shaped molecules fail to uniformly align in the presence of a quite strong $\vec{H}$ field. In principle, the macroscopic property χ_a in uniaxial LC phases is given by the product of the molecular property $\Delta\chi^{\rm mol}$ and the Saupe order parameter S as well as the number of molecules in the sample [31].

Among the three studied members of the PBBC series, 11ClPBBC and 10DClPBBC align with the director parallel to the $\vec{H}$ field of 9.4 T, while 10BrPBBC (or 10ClPBBC) does not seem to behave the same at the same field strength [32]. Perhaps the latter might likely be aligned with the directors perpendicular to the $\vec{H}$ field deep in the nematic phase. Given that $\Delta\chi^{\rm mol}$ is strictly dependent on the molecular conformation, the relevant MST parameters of 10DClPBBC, 11ClPBBC, and 10BrPBBC in different conformation Ω_i have been calculated and reported in Table III. It is clear from this table that $\Delta\chi^{\rm mol}$ and the asymmetric term $\eta_\chi^{\rm mol}$ are rather similar for the three studied PBBC members, especially taking into account possible averages over various conformational states. Hence, the reason behind the different alignment property of 10BrPBBC in the magnetic field from the other two members could be its conformational probability distribution being very different (as mentioned in Sec. III A) from those of 11ClPBBC and 10DClPBBC[2] (see Table I).

TABLE III. Molecular magnetic susceptibility tensor parameters (cgs-ppm) for the systems: 5CB, 5OCB (used for comparison), and the minimum energy conformers Γ_i, Σ_i, and Π_i for the 11ClPBBC, 10DClPBBC, and 10BrPBBC systems, respectively. χ_{ii} are the principal components, $\chi^{\rm iso}$ is the isotropic value, $\Delta\chi = \chi_{ZZ} - 1/2(\chi_{XX}+\chi_{YY})$ is the anisotropy part, and $\eta_\chi = \frac{\chi^0_{11}-\chi^0_{22}}{\chi^0_{33}}$ is the asymmetry term. Note that χ^0_{11}, χ^0_{22}, and χ^0_{33} are the principal components of the traceless MST, ordered according to the convention $|\chi_{33}-\chi^{\rm iso}| \geqslant |\chi_{22}-\chi^{\rm iso}| \geqslant |\chi_{11}-\chi^{\rm iso}|$. Additionally the above mentioned parameters were reported here also for the A131 [12], which has been recently claimed to form a biaxial nematic phase [5].

System	$\chi^{\rm mol}_{XX}$	$\chi^{\rm mol}_{YY}$	$\chi^{\rm mol}_{ZZ}$	$\chi^{\rm iso}$	$\Delta\chi^{\rm mol}$	$\eta_{\chi^{\rm mol}}$
5CB	−141.6	−224.8	−139.2	−168.5	40.4	0.04
5OCB	−154.3	−228.6	−144.9	−175.9	32.5	0.18
11ClPBBC (Γ_1)	−507.1	−658.3	−452.6	−539.4	130.1	0.46
11ClPBBC (Γ_2)	−469.9	−700.2	−452.9	−541.0	132.1	0.11
11ClPBBC (Γ_3)	−524.4	−644.2	−453.2	−540.6	131.1	0.70
11ClPBBC (Γ_4)	−507.2	−659.3	−454.6	−540.4	128.6	0.44
10DClPBBC (Σ_1)	−469.9	−700.2	−452.9	−541.0	132.1	0.11
10DClPBBC (Σ_2)	−470.9	−698.2	−456.9	−542.0	127.6	0.09
10DClPBBC (Σ_3)	−487.7	−681.6	−453.0	−540.8	131.6	0.24
10DClPBBC (Σ_4)	−471.9	−700.2	−448.0	−540.4	128.6	0.44
10BrPBBC (Π_1)	−486.0	−637.3	−439.3	−544.9	122.4	0.40
10BrPBBC (Π_2)	−481.2	−698.4	−458.7	−546.1	131.1	0.15
10BrPBBC (Π_3)	−502.8	−672.1	−462.3	−540.4	128.6	0.44
10BrPBBC (Π_4)	−490.4	−690.9	−454.7	−545.3	135.9	0.25
A131(Γ_1)	−509.4	−528.8	−350.6	−462.9	168.5	0.16
A131(Γ_2)	−438.3	−589.8	−367.7	−465.3	146.4	0.56
A131(Γ_3)	−437.9	−582.4	−373.7	−464.7	136.5	0.54
A131(Γ_4)	−511.7	−527.0	−349.8	−462.9	169.5	0.12

It is important to notice that the MSTs calculated for the full PBBC molecules in the most stable conformation, where an isotropic shift factor of ∼200 cgs-ppm has been applied owing to lengthening the aliphatic chains, are approximately the same as those obtained for the corresponding conformation in the 5R model (in general the aliphatic portions of the molecule do not alter the anisotropy but only the isotropic part of the MST). Generally, both the isotropic and anisotropic parts of the MST obtained for PBBC conformers are comparable with those calculated for another series of V-shaped molecules with similar molecular structures [29] and with those recently derived for A131 mesogen in different conformations [12]. Moreover, note that $\Delta\chi^{\rm mol}$ of the bent-core molecules (both PBBC and A131) is larger by a factor of about 4 when comparing with those of conventional uniaxial rodlike mesogens such as 5CB and 5OCB (see Table III).

[2]The probability distribution among the four low-lying conformers for each member of PBBC series was obtained albeit *in vacuo*. It is anticipated that among members in a homologous series, the relative behaviors in these probability distributions could also be altered due to different medium effects.

TABLE IV. ^{13}C chemical shift tensors (ppm), calculated at *in vacuo* GIAO-DFT [PBE1PBE/6-311+G(d,p)] level of theory on 2ClPBBC (Γ_1) minimum energy conformer and experimentally determined by 2D SUPER experiment on 11ClPBBC and related compounds.

	DFT					EXP					
	δ^{iso}	δ_{33}	δ_{22}	δ_{11}	γ	δ^{iso}	δ_{33}	δ_{22}	δ_{11}	γ	Ref.
C1	159.9	243.0	169.6	67.2	180.0	160.5	247.4	165.7	68.3	180.0	[45]
C2	111.8	198.5	125.6	11.3	118.3	111.2	192.3	126.0	15.4	120.0	[1]
C3	127.8	228.4	140.8	14.2	59.1	127.5	225.2	136.2	21.2	60.0	[1]
C4	132.0	219.0	161.8	15.2	0.0	127.5	229.0	144.9	8.6	0.0	[1]
C5	147.8	240.9	186.9	15.5	180.0	143.0	236.0	173.0	20.0	180.0	[46]
C6	124.9	223.6	137.4	13.7	119.7	126.6	204.6	140.7	34.4	120.0	[45]
C7	130.9	234.7	153.5	4.5	59.2	128.5	219.7	154.5	11.3	60.0	[1]
C8	124.5	216.0	134.5	23.1	0.0	126.1	223.7	127.4	27.3	0.0	[1]
C9	146.4	229.6	140.5	69.0	−119.2	144.9	217.2	145.2	72.2	−120.0	[45]
C10	127.6	201.0	119.6	62.4	176.5	122.4	213.6	109.0	44.6	180.0	[45]
C11	126.8	219.9	136.3	24.2	119.2	120.6	201.7	130.7	29.3	120.0	[1]
C12	117.7	202.2	140.4	10.4	59.8	114.8	189.6	124.2	30.7	60.0	[1]
C13	149.4	239.3	137.0	71.7	−2.1	146.0	249.3	129.9	58.9	0.0	[1]
C14	113.9	184.2	137.3	20.3	−59.2	120.8	183.0	149.3	30.0	−60.0	[45]
C15	124.6	216.7	135.1	22.1	0.0	126.1	223.7	127.4	27.3	0.0	[1]
C16	130.5	234.4	152.7	4.4	60.5	128.5	219.7	154.5	11.3	60.0	[1]
C17	124.9	223.7	137.4	13.7	120.1	126.6	204.6	140.7	34.4	120.0	[45]
C18	147.7	240.9	186.6	15.5	180.0	143.0	236.0	173.0	20.0	180.0	[46]
C19	132.1	219.2	162.1	14.9	0.0	127.5	229.0	144.9	8.6	0.0	[1]
C20	127.8	228.5	140.8	14.2	60.2	127.5	225.2	136.2	21.2	60.0	[1]
C21	111.8	198.5	125.6	11.2	120.4	111.2	192.3	126.0	15.4	120.0	[1]
C22	159.9	243.0	169.6	67.0	180.0	160.5	247.4	165.7	68.3	180.0	[45]
Z1	162.5	265.2	120.2	102.1	−33.7	163.8	267.8	117.1	106.6	−30.0	[3]
Z2	163.2	265.3	118.3	106.0	−32.4	163.8	267.8	117.1	106.6	−30.0	[3]

D. ^{13}C chemical shielding tensor and NMR analyses

The quantum mechanical methodologies have now matured to such an extent that the results of *ab initio* calculations can significantly enhance the interpretative power of NMR spectra obtained from different types of liquid crystalline systems [2,3,33–41]. In particular, recent developments in *ab initio* methods and computer hardware have made accurate evaluation of ^{13}C NMR chemical shieldings of many molecular systems possible. The CSTs calculated using fully relaxed minimum energy structures of the 5R models from the *in vacuo* GIAO-DFT [PBE1PBE/6-311+G(d,p)] method for 2ClPBBC (Γ_1), 2DClPBBC (Σ_2), and 2BrPBBC (Π_1) are reported in Tables IV, V, and VI, respectively.

Moreover, the calculated *in vacuo* GIAO-DFT CSTs of PBBC models employing the other three functionals (B1LYP, B3PW91, and MPW1PW91) are reported in Tables I, II, and III of the supplementary material [42]. In all three molecular models, the PBE1PBE functional is the most reliable functional for obtaining ^{13}C CSTs, giving the lowest absolute residuals for both the isotropic value (δ_{iso}) and $\langle\delta\rangle$, the mean principal components (δ_{ii}, with $ii = 11,22,33$), averaged over all the relevant carbons as summarized in Table VII. (The MPW1PW91 functional gives CSTs comparable to those calculated with the PBE1PBE functional, while the Becke one-parameter hybrid functional B1LYP is revealed to be the worst one. The B3PW91 collocates between the MPW1PW91 and the B1LYP.) Figure 6 shows radial plots of δ_{iso} and $\langle\delta_{ii}\rangle = (\delta_{11} + \delta_{22} + \delta_{33})/3$ for various carbon sites of 2ClPBBC (Γ_1), 2DClPBBC (Σ_2), and 2BrPBBC (Π_1) (the absolute residual for each principal component, δ_{11},δ_{22}, and δ_{33}, is reported in the supplementary material [42]). The DFT functional used nowadays for the determination of CSTs introduces larger deviations for heavy atoms (e.g., chlorine or bromine) when comparing to those for ^{13}C. Furthermore, from the experimental point of view, the CSA powder patterns recorded for the halogen-bonded quaternary carbons show both lower signal-to-noise ratio and spectral resolution compared to those determined for the C-H and C-C carbons. This indicates that the experimental CSAs for carbons C10, C11, C12, and C13 must be taken with some caution. Moreover, the relative values of CSA components found for these carbons have the largest deviations from those commonly found in carbons having the same topology and chemical nature [43].

The root-mean-squared deviation evaluated among the Γ_i, Σ_i, and Π_i conformers (data not shown) is about $\pm$1.2 ppm for all the conformations, showing that there are no significant dependencies of the CSA tensors on the different conformational states as seen in A131 [2]. The average absolute residual for δ_{iso} of the three PBBC models obtained from EXP and DFT ranges between 0.2 and 1.6 ppm and agrees well with the average experimental uncertainty deviations ($\sim$0.8 ppm). The accuracy of each CSA component evaluated from 2D SUPER powder patterns of PBBC mesogens is about $\pm$4–6 ppm, which is lower than the mean absolute residuals $\langle\delta\rangle$ determined in the comparison between the experimental

TABLE V. ^{13}C chemical shift tensors (ppm), calculated at *in vacuo* GIAO-DFT [PBE1PBE/6-311+G(d,p)] level of theory on 2DClPBBC (Σ_2) minimum energy conformer and experimentally determined by 2D SUPER experiment on 10DClPBBC and related compounds. References of EXP are those in Table IV.

	DFT					EXP				
	δ^{iso}	δ_{33}	δ_{22}	δ_{11}	γ	δ^{iso}	δ_{33}	δ_{22}	δ_{11}	γ
C1	157.6	237.8	169.0	66.1	180.0	160.5	247.4	165.7	68.3	180.0
C2	111.1	195.5	126.7	11.0	119.4	111.2	192.3	126.0	15.4	120.0
C3	127.2	225.3	141.9	14.3	58.8	127.5	225.2	136.2	21.2	60.0
C4	130.8	215.9	161.6	14.9	0.0	127.5	229.0	144.9	8.6	0.0
C5	146.3	237.8	186.2	15.1	180.0	143.0	236.0	173.0	20.0	180.0
C6	124.3	221.0	138.4	13.5	119.2	126.6	204.6	140.7	34.4	120.0
C7	130.1	231.5	154.2	4.6	57.6	128.5	219.7	154.5	11.3	60.0
C8	122.9	212.1	134.2	22.3	0.0	126.1	223.7	127.4	27.3	0.0
C9	142.3	221.0	139.5	66.4	−119.3	144.9	217.2	145.2	72.2	−120.0
C10	128.0	199.2	124.1	60.7	179.5	122.4	213.6	109.0	44.6	180.0
C11	126.3	209.0	130.0	39.9	121.2	120.6	201.7	130.7	29.3	120.0
C12	128.0	199.3	124.1	60.7	58.8	122.4	213.6	109.0	44.6	60.0
C13	142.3	221.1	139.3	66.5	0.5	146.0	249.3	129.9	58.9	0.0
C14	117.3	186.4	149.0	16.4	−60.2	120.8	183.0	149.3	30.0	−60.0
C15	122.9	212.2	134.2	22.3	0.0	126.1	223.7	127.4	27.3	0.0
C16	130.1	231.5	154.2	4.6	57.6	128.5	219.7	154.5	11.3	60.0
C17	124.3	221.0	138.4	13.5	119.2	126.6	204.6	140.7	34.4	120.0
C18	146.3	237.8	186.2	15.1	180.0	143.0	236.0	173.0	20.0	180.0
C19	130.8	215.9	161.7	14.9	0.0	127.5	229.0	144.9	8.6	0.0
C20	127.2	225.3	141.9	14.3	58.8	127.5	225.2	136.2	21.2	60.0
C21	111.1	195.5	126.7	11.0	119.4	111.2	192.3	126.0	15.4	120.0
C22	157.6	237.7	169.0	66.1	180.0	160.5	247.4	165.7	68.3	180.0
Z1	158.1	258.8	118.9	96.4	−34.5	163.8	267.8	117.1	106.6	−30.0
Z2	158.1	258.8	118.9	96.6	−32.3	163.8	267.8	117.1	106.6	−30.0

and the PBE1PBE chemical shift tensor's components (see Table VII). In view of larger uncertainty in CSAs of some carbons mentioned above, the mean absolute residual has been also evaluated for a reduced set of carbons $\langle\delta\rangle_{red}$, namely by excluding those (C9, C10, C11, C12, C13, C14) located in the central ring C, which show the largest deviations from the experimental values. The evaluated $\langle\delta\rangle_{red}$ ranges between 5.4 and 6.5 ppm, which satisfactorily agrees with the above-mentioned experimental deviation. However, experimental CSAs were determined in the solid phase, while the DFT calculations were performed *in vacuo*, which did not account for the effect of molecular packing in the mesophase. Although carbon 13 is likely not to be affected by the packing effects, this is only partially true for the halogen-bonded carbons, which are indirectly influenced by the effect of the environment through the highly polarizable halogens atoms [37]. It is noticed that the orientations of the principal axis systems (PAS) of all the CSTs in different conformations are close to those expected from the standard geometry (e.g., the β angle for a protonated carbon on a phenyl ring is 60°) to within 2–4 degrees [3].

To illustrate the effects of using verified experimental (EXP) CSA tensors, we reexamine here the ^{13}C NMR results of 11ClPBBC [44]. Figure 7 reproduces EXP δ's for the aromatic region and X10 and X11 together with the correct peak assignment based on the EXP and GIAO-DFT CSA tensors listed in Table IV. Since 11ClPBBC has a monosubstituted chlorine on the central ring, the unprimed fragment refers to the biphenyl attached closer to the chlorine substituent. We use the EXP chemical shift tensors to analyze the δ from carbons 10, 14 of the central ring, and from carbons 1–8 of the "unprimed" and "primed" biphenyl fragments to get their local order parameters. Now, the CSA tensor's PAS (1,2,3) is chosen with its 3-axis along a C-H bond, or C-C bond (along the para axis direction), and the 1-axis normal to a ring plane [see Fig. 1(b)].

The local order parameters S and Δ of each ring are found from the observed ^{13}C shifts δ in a ring fragment according to [9]:

$$\delta = \delta_{iso} + \tfrac{2}{3}S\big[P_2(\cos\beta)(\delta_{33}-\delta_{22}) + \tfrac{1}{2}(\delta_{22}-\delta_{11})\big] + \tfrac{1}{3}\Delta[\delta_{11}-\delta_{22}\cos^2\beta-\delta_{33}\sin^2\beta], \quad (1)$$

where β, the angle between the orientation of δ_{33} of a particular carbon with the z' axis of the ring, is equal to 0 for quaternary carbons (carbon 1, 4, 5, 8) and 60° for protoned carbons (carbon 2, 3, 6, 7). The use of the regular geometry appears to be reasonable [36]. For the rings in the biphenyl fragment, the same S has been used. Now S represents the local nematic order of the para axis, and Δ represents the local biaxial ordering ($S_{xx}-S_{yy}$) with respect to the (x',y',z') frame [see Fig. 1(b)]. Note that since the central ring cannot flip about the z axis, the above equation should include also S_{xz}, which fortunately turns out to be negligible [2]. Thus, Eq. (1) is used for C10 and C14, where $\beta = 90°$ for C14 and $\beta = 150°$ for C10. Note here S denotes the nematic order of the z axis on the central ring.

TABLE VI. ^{13}C chemical shift tensors (ppm), calculated at *in vacuo* GIAO-DFT [PBE1PBE/6-311+G(d,p)] level of theory on 2BrPBBC (Π_1) minimum energy conformer and experimentally determined by 2D SUPER experiment on 10BrPBBC and related compounds. In this system the same powder pattern was assigned to C3, C6, C10, and C11 due to poor spectral resolution.

	DFT					EXP					
	δ^{iso}	δ_{33}	δ_{22}	δ_{11}	γ	δ^{iso}	δ_{33}	δ_{22}	δ_{11}	γ	Ref.
C1	159.9	242.0	171.0	66.7	180.0	160.5	247.4	165.7	68.3	180.0	[45]
C2	112.6	201.7	125.1	11.0	119.8	111.2	192.3	126.0	15.4	120.0	[1]
C3	128.3	230.7	140.2	14.0	58.9	127.5	225.2	136.2	21.2	60.0	[1]
C4	132.8	218.6	164.6	15.3	0.0	127.1	219.3	147.4	14.6	0.0	[47]
C5	147.1	239.8	186.9	14.6	180.0	143.0	236.0	173.0	20.0	180.0	[46]
C6	125.0	225.6	136.4	13.0	121.2	127.5	225.2	136.2	21.2	120.0	[1]
C7	131.7	237.4	153.6	4.1	60.3	131.0	240.6	151.7	0.7	60.0	[1]
C8	125.5	216.0	137.5	23.0	0.0	126.1	223.7	127.4	27.3	0.0	[1]
C9	149.7	238.9	139.8	70.6	−119.4	144.9	217.2	145.2	72.2	−120.0	[45]
C10	124.1	199.7	112.9	59.6	179.2	127.5	225.2	136.2	21.2	180.0	[1]
C11	131.4	229.3	136.1	28.6	120.6	127.5	225.2	136.2	21.2	120.0	[1]
C12	118.7	204.8	139.8	11.6	60.3	121.2	220.9	137.7	5.1	60.0	[1]
C13	150.2	238.4	141.0	71.2	2.1	146.0	249.3	129.9	58.9	0.0	[1]
C14	116.2	189.0	136.8	22.6	−60.9	120.8	183.0	149.3	30.0	−60.0	[45]
C15	126.2	216.7	138.4	23.3	0.0	126.1	223.7	127.4	27.3	0.0	[1]
C16	130.8	236.7	152.9	2.8	58.8	131.0	240.6	151.7	0.7	60.0	[1]
C17	126.0	225.6	136.8	15.4	121.2	127.5	225.2	136.2	21.2	120.0	[1]
C18	148.4	241.1	189.7	14.4	180.0	143.0	236.0	173.0	20.0	180.0	[46]
C19	130.9	218.3	162.2	12.2	0.0	127.1	219.3	147.4	14.6	0.0	[47]
C20	128.1	230.4	139.9	14.2	58.3	127.5	225.2	136.2	21.2	60.0	[1]
C21	112.3	201.3	125.0	10.6	120.4	111.2	192.3	126.0	15.4	120.0	[1]
C22	159.9	242.2	170.8	66.6	180.0	160.5	247.4	165.7	68.3	180.0	[45]
Z1	162.3	263.7	119.0	104.1	−35.6	163.8	267.8	117.1	106.6	−30.0	[3]
Z2	162.7	263.3	118.2	106.8	−34.2	163.8	267.8	117.1	106.6	−30.0	[3]

As done before [1], we use the Haller equation for S, viz., $S(T) = S_0(1 - T/T^*)^f$, where S_0 and f are empirical constants and T^* ($T^* = T_c + 1$ K) is the temperature slightly above T_c at which S vanishes, and Δ with a linear temperature dependence, i.e., $\Delta = \alpha(T - T_c)$, where α is a fitting constant. The local order parameters for the central phenyl ring and biphenyl fragments are, therefore, obtained by optimizing the fittings between the calculated and experimental δ's, and the calculated δ's are shown as solid lines in Fig. 7. The derived local S and Δ values of the central ring and biphenyl groups are plotted versus temperature also in this figure. These results imply that the local z axis located on the central ring represents a more ordered axis and coincides with the long molecular axis, thereby reflecting the overall molecular ordering. The ordering of the local z' and z axes are related by $S' = SP_2(\cos\beta_F)$, where β_F, the angle between the para axes of the biphenyl group (S') and the more ordered z axis (S), can be found. Consequently, the bend angle is estimated to vary from 127° to 129° upon decreasing temperature (see Fig. 8). The bend angles found in DFT optimized structures (see Table I) belong to two groups (Γ_1, Γ_4) and (Γ_2, Γ_3). The former has a value of about 123°, while the value of the latter is about 130°. Indeed, when comparing these with the NMR derived bend angle, the trend of experimental bend angle seems to suggest that the higher energy ones Γ_2, Γ_3 ($\Theta_{EXP} \sim 129°$, $\Theta_{DFT} \sim 130°$) could become more populated at the the expense of the lower energy DFT structures Γ_1, Γ_4. It is interesting to also note that among the phenyl rings A and B, their Δ values are similar and of the same sign, while for the D and E rings in the other biphenyl fragment their Δ's are of opposite sign, implying that there is a more pronounced twist than that between A and B. This is in agreement with the structural features that came out from the DFT calculations.

The results from the analysis of 10DClPBBC can be found in the supplementary material [42]. The twist between the D and E rings in 11ClPBBC is not seen in 10DClPBBC as there is no significant twist between ring planes in the biphenyls (see supplemental information). However, the Δ of the central ring has positive values, while the rings in the biphenyls have neg-

TABLE VII. Mean absolute residuals (ppm) for δ_{iso} and for $\langle\delta\rangle$ ($\langle\delta\rangle_{red}$), the mean of principal components (δ_{ii}, with $ii = 11,22,33$), averaged over all the relevant carbons in the low-energy conformers of 2ClPBBC (Γ_1), 2DClPBBC (Σ_2), and 2BrPBBC (Π_1).

		B1LYP	B3PW91	MPW1PW91	PBE1PBE
2ClPBBC[Γ_1]	δ_{iso}	7.1	3.4	2.5	1.1
	$\langle\delta\rangle$	11.3	9.2	8.8	7.9
	$\langle\delta\rangle_{red}$	9.2	6.9	6.5	5.4
2DClPBBC[Σ_2]	δ_{iso}	7.7	4.0	3.0	0.2
	$\langle\delta\rangle$	11.0	8.8	8.4	7.9
	$\langle\delta\rangle_{red}$	9.3	7.2	6.7	6.5
2BrPBBC[Π_1]	δ_{iso}	6.2	2.5	0.7	1.6
	$\langle\delta\rangle$	9.9	8.1	7.5	7.7
	$\langle\delta\rangle_{red}$	8.0	5.9	5.3	5.5

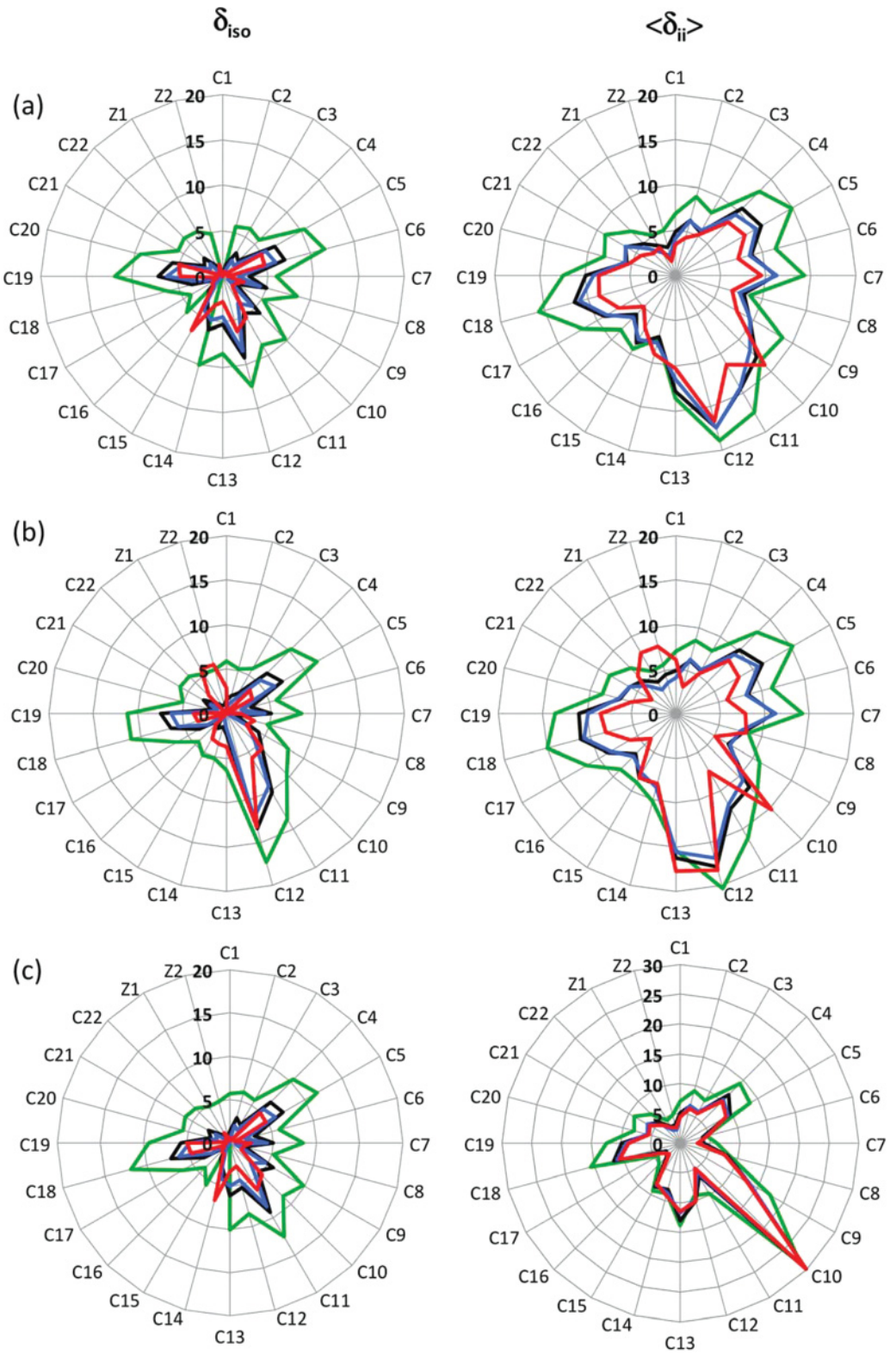

FIG. 6. (Color online) Absolute residuals for the isotropic shift (δ_{iso}) and the average of the three principal components (δ_{33}, δ_{22}, δ_{11}) of the ^{13}C chemical shielding tensors belonging to the different systems: (a) 2ClPBBC (Γ_1), (b) 2DClPBBC (Σ_2), and (c) 2BrPBBC (Π_1). The absolute residuals are calculated with respect to the experimental values reported in Tables IV, V, and VI. The green, black, blue, and red colors refer to the B1LYP, B3PW91, MPW1PW91, and PBE1PBE functionals used in the DFT calculations, respectively.

ative Δ values, implying that the central ring plane is twisted in the opposite direction with respect to those of the biphenyls. The twist conformation in V-shaped molecules depends, therefore, on the specific substitution in the central ring. The bend angle Θ of 10DClPBBC depends on temperature, ranging from 132° to 123° at the low-temperature end (see Fig. 8).

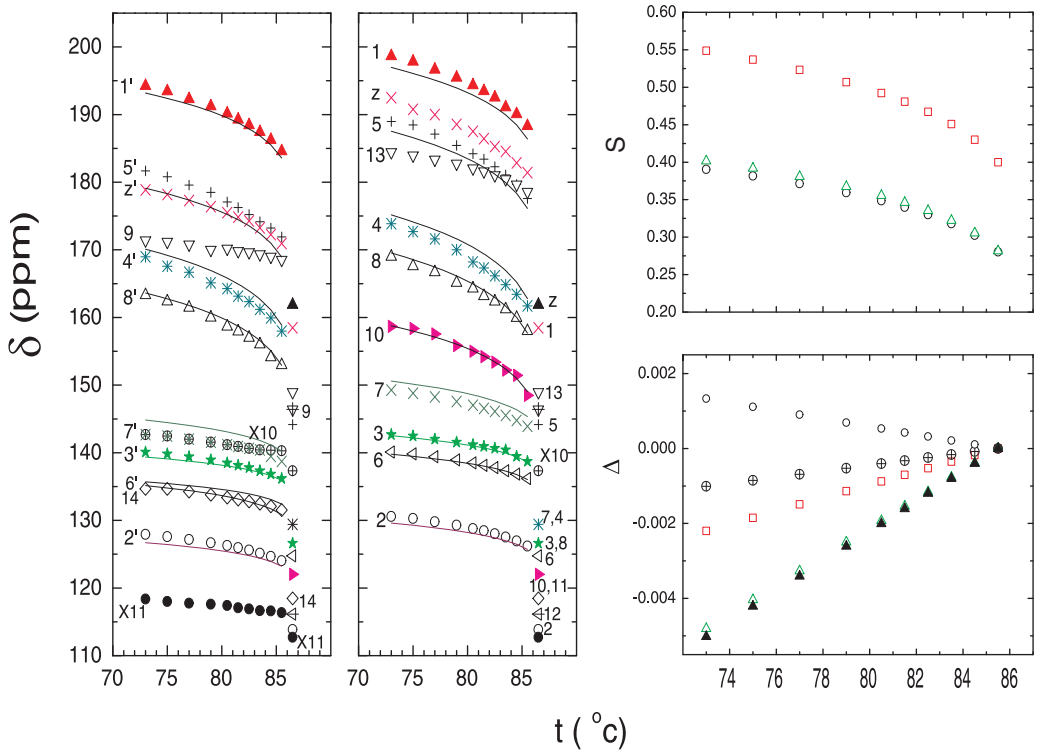

FIG. 7. (Color online) Left: Plots of $\langle\delta\rangle$ for the aromatic carbons and aliphatic carbons X10 and X11 in the *I* and *N* phases of 11ClPBBC. The carbon labels are indicated in Fig. 1. While the unprimed labels refer to biphenyl fragment attached closer to the chlorine substituent, the prime carbon labels refer to the other biphenyl fragment. Solid curves denote calculated $\langle\delta\rangle$'s. Right: Plot of the local order parameters S and Δ versus temperature for the biphenyl fragments (triangles for "unprimed" fragment, circles for "primed" fragment) and center ring (squares) in the *N* phase of 11ClPBBC (solid triangles for phenyl ring closer to the center ring, and open symbols for the outer phenyl ring in the biphenyl group). S_0 and f, in the Haller equation, for the unprimed and primed biphenyl groups and central ring are given by (0.6722, 0.1587), (0.6318, 0.1483), and (0.8689, 0.1416), respectively.

When comparing with the angles found by DFT in Table I, the lowest energy conformations Σ_2 and Σ_3 are populated at high temperature ($\Theta_{EXP} \sim 132^\circ$, $\Theta_{DFT} \sim 130^\circ$), while Σ_1 and Σ_4 seem to become populated at low temperatures ($\Theta_{EXP} \sim 123^\circ$, $\Theta_{DFT} \sim 122^\circ$), even though these are not allowed *in vacuo*. This necessarily points to the fact that in condensed phases the packing effect can change the conformational landscape of V-shaped molecules. This implies that in reality the *in vacuo* DFT predicted conformations having higher energies and lower populations can also be favored. This finding has also been seen in the A131 mesogen, where a conformational change from the N_u ($\Theta_{EXP} = 153^\circ$–163°, $\Theta_{DFT} \sim 145^\circ$) to the N_b ($\Theta_{EXP} = 111^\circ$–129°, $\Theta_{DFT} \sim 115^\circ$) phase was observed via a change in the bend angle within the nematic range. In general, the observed conformational change is consistent with the DFT prediction of several distinct conformational states for the bent-core region in nematic forming V-shaped mesogens.

IV. SUMMARY

The methodologies of DFT have been used to aid the interpretation of ^{13}C solid state NMR results, to evaluate theoretical IR spectra and MSTs of several members of a PBBC homologous series. In searching the energy surface landscape, DFT calculated configurations are found to be useful in pinpointing possible conformation states for the bent-core region of the V-shaped molecule. Such optimized molecular structures are used to evaluate CSAs of various carbon sites, using different possible functionals. It is found that the PBE1PBE functional performs the best in giving the

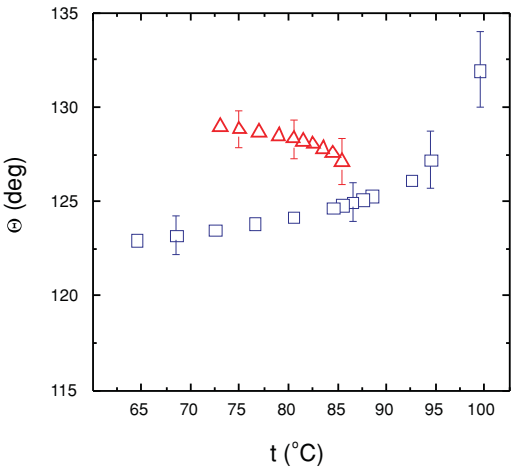

FIG. 8. (Color online) Plot of the bend angle versus temperature in the uniaxial nematic phase of 10DClPBBC (squares) and of 11ClPBBC (triangles).

CSAs when compared with the experimentally determined CSTs. Moreover, the calculated CSAs are found to be insensitive to the different possible conformational states in each PBBC member. IR spectra and MSTs have been calculated for three 5R minimum energy models: (a) 2ClPBBC (Γ_1), (b) 2DClPBBC (Σ_2), and (c) 2BrPBBC (Π_1). It is noted that certain vibration modes would be valuable as a complementary technique to ^{13}C NMR in obtaining ordering information in PBBC series. The MSTs found for different conformers are different, but taking into account conformational averaging among them, the average MST of the three members of PBBC series cannot be clearly distinguished. Thus, these calculated MSTs could provide a clue to how V-shaped mesogens in a homologous series can orient in the external $\vec{H}$ field. Indeed, the substitution on the central ring and the chain length have been found to have a profound effect on the alignment of the PBBC bent-core molecules in the $\vec{H}$ field. The alignment difficulty of V-shaped molecules in the magnetic field has also been noted by other researchers. The reason behind this remains an important open question.

Finally, the NMR Θ angle may be interpreted as a configuration-averaged angle between the two lateral wings in the PBBC bent-core molecule. Also, a twisted conformation for the bent core can be inferred in PBBC series from the local molecular biaxiality Δ's, and the details in the orientations of ring planes depend on the substitution at the central ring. The bend angle and the choice of molecular structure in the bent-core region may ultimately determine the occurrence of a biaxial nematic phase before the crystallization sets in. Both the PBBC series and A131 studied using the current approach strongly support the notion that lowly populated conformational states found *in vacuo* by DFT can be reached in real mesogens upon decreasing temperature due to collective packing of molecules in the condensed phase.

ACKNOWLEDGMENTS

R.Y.D. thanks the Natural Sciences and Engineering Council of Canada for financial support, and A.M. is particularly grateful to Professor Benedetta Mennucci and to Professor C. A. Veracini for useful discussions.

[1] R. Y. Dong, J. Phys. Chem. B **113**, 1933 (2009).
[2] R. Y. Dong and A. Marini, J. Phys. Chem. B **113**, 14062 (2009).
[3] A. Marini, V. Prasad, and R. Y. Dong, in *Nuclear Magnetic Resonance Spectroscopy of Liquid Crystals*, edited by R. Y. Dong (World Scientific Publishing Co., Singapore, 2009), Chap. 13.
[4] H. G. Yoon, S.-W. Kang, R. Y. Dong, A. Marini, K. A. Suresh, M. Srinivasarao, and S. Kumar, Phys. Rev. E **81**, 051706 (2010).
[5] V. Prasad, S.-W. Kang, K. A. Suresh, L. Joshi, Q. Wang, and S. Kumar, J. Am. Chem. Soc. **127**, 17224 (2005).
[6] T. Niori, F. Sekine, J. Watanabe, T. Furukawa, and H. Takezoe, J. Mater. Chem. **6**, 1231 (1996).
[7] D. A. Dunmur and K. Toriyama, in *Physical Properties of Liquid Crystals*, edited by D. Demus, J. Goodby, G. W. Gray, H. W. Spiess, and V. Vill (Wiley-VHC, Weinheim, 1999).
[8] J. L. Figueirinhas, G. Feio, C. Cruz, M. Lehmann, C. Köhn, and R. Y. Dong, J. Chem. Phys. **133**, 174509 (2010).
[9] R. Y. Dong, J. Xu, J. Zhang, and C. A. Veracini, Phys. Rev. E **72**, 061701 (2005).
[10] P. I. C. Teixeira, A. J. Masters, and B. M. Mulder, Mol. Cryst. Liq. Cryst. **323**, 167 (1998).
[11] G. R. Luckhurst, Thin Solid Films **393**, 40 (2001).
[12] A. Marini and R. Y. Dong, Mol. Cryst. Liq. Cryst. **525**, 74 (2010).
[13] M. J. Frisch *et al.*, *Gaussian 03* (Rev. E.05) (Gaussian, Inc., Wallingford, CT, 2004).
[14] K. B. Wiberg, J. Comput. Chem. **20**, 1299 (1999).
[15] A. D. Becke, Phys. Rev. A **38**, 3098 (1988).
[16] C. Lee, W. Yang, and R. G. Parr, Phys. Rev. B **37**, 785 (1988).
[17] P. J. Stephens, F. J. Devlin, C. H. Chabalowski, and M. Frisch, J. Phys. Chem. **98**, 11623 (1994).
[18] R. Ditchfield, J. Chem. Phys. **56**, 5688 (1972).
[19] R. Wrzalik, K. Merkel, and A. Kocot, J. Mol. Model. **9**, 248 (2003).
[20] C. Adamo and V. Barone, Chem. Phys. Lett. **274**, 242 (1997).
[21] A. D. Becke, J. Chem. Phys. **98**, 5648 (1993).
[22] J. P. Perdew and Y. Wang, Phys. Rev. B **45**, 13244 (1992).
[23] C. Adamo and V. Barone, J. Phys. Chem. A**108**, 664 (1998); B. J. Lynch, Y. Zhao, and D. G. Truhlar, J. Phys. Chem. A **107**, 1384 (2003).
[24] C. Adamo and V. Barone, J. Chem. Phys. **110**, 6158 (1999).
[25] L. Calucci, C. Forte, K. Fodor-Csorba, B. Mennucci, and S. Pizzanelli, J. Phys. Chem. B **111**, 53 (2007).
[26] J. P. Merrick, D. Moran, and L. Radom, J. Phys. Chem. A **111**, 11683 (2007).
[27] K. Merkel, A. Kocot, J. K. Vij, G. H. Mehl, and T. Meyer, J. Chem. Phys. **121**, 5012 (2004).
[28] V. Domenici, C. A. Veracini, and B. Zalar, Soft Matter **1**, 408 (2005).
[29] V. Domenici, C. A. Veracini, K. Fodor-Csorba, G. Prampolini, I. Cacelli, A. Lebar, and B. Zalar, ChemPhysChem **8**, 2321 (2007).
[30] P. G. de Gennes and J. Prost, in *The Physics of Liquid Crystals* (Clarendon, New York, 1993), pp. 57-58.
[31] A. Saupe and G. Englert, Mol. Cryst. **1**, 503 (1966).
[32] R. Y. Dong, J. Zhang, and K. Fodor-Csorba, Chem. Phys. Lett. **417**, 475 (2006). The reported CSA tensors are unfortunately incorrect, and some are assigned to the wrong carbons.
[33] D. Catalano, M. Geppi, A. Marini, C. A. Veracini, S. Urban, J. Czub, W. Kuczynski, and R. Dabrowski, J. Phys. Chem. C **111**, 5286 (2007).
[34] M. Geppi, A. Marini, C. A. Veracini, S. Urban, J. Czub, W. Kuczynski, and R. Dabrowski, J. Phys. Chem. B **112**, 9663 (2008).
[35] S. Borsacchi, L. Calucci, J. Czub, R. Dabrowski, M. Geppi, W. Kuczyski, A. Marini, B. Mennucci, and S. Urban, J. Phys. Chem. B **113**, 15783 (2009).

[36] R. Y. Dong, M. Geppi, A. Marini, V. Hamplova, M. Kaspar, C. A. Veracini, and J. Zhang, J. Phys. Chem. B **111**, 9787 (2007).

[37] A. Marini, *Understanding Complex Liquid Crystalline Materials: A Multinuclear NMR Spectroscopy and Ab Initio Calculations Approach* (VDM Verlag Dr. Muller Aktiengesellschaft & Co. KG, Saarbrücken, Germany, 2010).

[38] L. Calucci, M. Geppi, A. Marini, and C. A. Veracini, Phys. Rev. E **82**, 041702 (2010).

[39] A. Marini and V. Domenici, J. Phys Chem. B **114**, 10391 (2010).

[40] A. Marini and V. Domenici, Ferroelectrics **395**, 46 (2010).

[41] M. Cifelli, V. Domenici, A. Marini, and C. A. Veracini, Liq. Cryst. **37**, 935 (2010).

[42] See supplemental material at [http://link.aps.org/supplemental/10.1103/PhysRevE.83.041712] for absolute residuals of the ^{13}C chemical shift principal components evaluated in PBBC molecules; observed ^{13}C chemical shift $\langle\delta\rangle$ and derived local principal (S) and local biaxial (D) order parameter relative to 10DClPBBC; and ^{13}C chemical shift tensors for 2ClPBBC (Γ_1), 2DClPBBC (Σ_3), and 2BrPBBC (Π_1) calculated at GIAO-DFT level of theory.

[43] T. M. Duncan, *Principal Components of Chemical Shielding Tensors: A Compilation*, 2nd ed. (Farragut Press, Madison, WI, 1997).

[44] R. Y. Dong, J. Xu, G. Benyei, and K. Fodor-Csorba, Phys. Rev. E **70**, 011708 (2004).

[45] J. Xu, K. Fodor-Csorba, and R. Y. Dong, J. Phys. Chem. A **109**, 1998 (2005).

[46] T. Nakai, H. Fujimori, D. Kuwahara, and S. Miyajima, J. Phys. Chem. B **103**, 417 (1999).

[47] G. Zheng, J. Hu, X. Zhang, L. Shen, C. Ye, and G. A. Webb, J. Mol. Struct. (THEOCHEM) **428**, 283 (1998).